Scattering strength dependence of terahertz random lasers

Cite as: J. Appl. Phys. **125**, 151611 (2019); https://doi.org/10.1063/1.5083699
Submitted: 30 November 2018 . Accepted: 04 March 2019 . Published Online: 03 April 2019

S. Schoenhuber, M. Wenclawiak, M. A. Kainz, B. Limbacher, A. M. Andrews, H. Detz, G. Strasser, J. Darmo, and K. Unterrainer

Journal of Applied Physics ARTICLE scitation.org/journal/jap

Scattering strength dependence of terahertz random lasers

Cite as: J. Appl. Phys. **125**, 151611 (2019); doi: 10.1063/1.5083699
Submitted: 30 November 2018 · Accepted: 4 March 2019 ·
Published Online: 3 April 2019

S. Schoenhuber,[1,2,a)] M. Wenclawiak,[1,2] M. A. Kainz,[1,2] B. Limbacher,[1,2] A. M. Andrews,[2,3] H. Detz,[2,4] G. Strasser,[2,3] J. Darmo,[1,2] and K. Unterrainer[1,2]

AFFILIATIONS

[1]Photonics Institute, TU Wien, 1040 Vienna, Austria
[2]Center for Micro- and Nanostructures, TU Wien, 1040 Vienna, Austria
[3]Institute for Solid-State Electronics, TU Wien, 1040 Vienna, Austria
[4]Central European Institute of Technology, Brno University of Technology, 61200 Brno, Czech Republic

[a)]**Electronic mail:** sebastian.schoenhuber@tuwien.ac.at

ABSTRACT

Random lasing operation requires an active region, a gain medium that supports multiple scattering, and, especially for integrated optoelectronic devices, a nonresonant outcoupling mechanism over a continuous spectrum. For broadband operation, the resonator geometry must provide frequency nonselective, strong feedback over a large bandwidth. The feedback mechanism by multiple scattering in terahertz semiconductor random lasers and the bandwidth of such cavities are presented and discussed. We demonstrate the influence of shape and scattering strength of the scatterers on the lasing process and determine the bandwidth of such resonator structures. We use passive resonator structures to prove that the feedback as well as the outcoupling is frequency independent over a large bandwidth.

I. INTRODUCTION

Since their first demonstration, terahertz (THz) quantum cascade lasers (QCLs) underwent an unprecedented development. Lasing frequencies ranging from 1.2 to 5.4 THz[1,2] with individual active regions covering more than one octave in frequency for comb operation,[3] output powers up to 2.4 W in a pulsed[4] operation and 230 mW in a continuous-wave[5] operation, and a maximum operating temperature of 199.5 K[6] were reached. In recent years, several cavity concepts have been developed to provide the desired emission characteristics and beam shapes for spectroscopic and imaging applications. The resonator, structured in one dimension using distributed feedback (DFB) gratings[7] of an even or odd order, is used to create a single mode emission with a narrow far field, and wire lasers[8] provide a highly efficient cavity with low divergence. Two-dimensional texturing of the cavity in the shape of photonic crystals,[9] quasiperiodic Penrose,[10] or hyperuniform patterns[11] provides control of the lasing modes and subsequently of the emission properties. By carefully designing grating parameters and periodicity, a specific optical mode with the desired characteristics can be selected. Recently, several reports demonstrated the application of random feedback mechanisms. Disordered arrays of dielectric, metallic and etched air hole pillars were applied to electrically injected lasers and led to a multimode emission over a large bandwidth with a collimated far field[12–14] and low-spatial coherence. These emission properties can be exploited for speckle-free imaging applications.[15,16] Also, physical phenomena like the Anderson localization of light can be observed[17] in the systems with a random feedback mechanism. Understanding the multiple scattering feedback mechanisms is necessary for the further development of these cavity concepts. However, an accurate analysis of the mode formation process inside random cavities using finite element or finite difference time domain methods is challenging. Nonlinear effects[18] including spatial hole burning[19] and gain competition between individual cavity modes cannot be taken into account due to the required huge computational effort. An experimental investigation of the frequency range of the random laser feedback mechanism is challenging since the observed emission spectrum presents only the modes with the lowest loss (the highest mode Q-factor). In this paper, we want to address the following two questions: (1) What is the bandwidth of the multiple scattering feedback mechanism, and

is it frequency selective? (2) Are modes in semiconductor random lasers formed by multiple-photon scattering? To answer these questions, we decouple the active region and the optical resonator. This enables the study of the bandwidth of the feedback mechanism without influence from nonlinear effects like gain competition. Separately, we study the crucial scattering strength of the multiple-photon scattering using active laser devices. In combination, our results allow a better understanding of the feedback mechanism which is important for the development of improved random laser cavities in order to optimize the feedback efficiency over a broad spectral range, leading to a source with a low-spatial coherence.

II. BANDWIDTH OF RANDOM RESONATORS

The bandwidth of the feedback depends on the resonator geometry. By calculating the two-dimensional Fourier transformation, the Fourier space $|\epsilon(k)|$ containing the supported k-vectors of a geometry is determined. As depicted in Fig. 1, an ordered structure, here in the shape of a lattice [Fig. 1(a)], supports discrete k-vectors [Fig. 1(b)]. For active laser devices, such a structure therefore supports discrete, selected modes only. If the structure has no underlying order but consists of an arrangement of randomly placed scatterers [Fig. 1(c)], the Fourier space contains a quasicontinuous k-space [Fig. 1(d)]. Therefore, an active structure supports quasi-continuously all modes within the feedback bandwidth. However, as seen in Fig. 1(d), this k-space is not infinite but limited by the shape of the scatterers. To study the influence of the scatterer radius, we calculate $|\epsilon(k)|$ for an ensemble of scatterers with random, but fixed positions and varied scatter radii. As

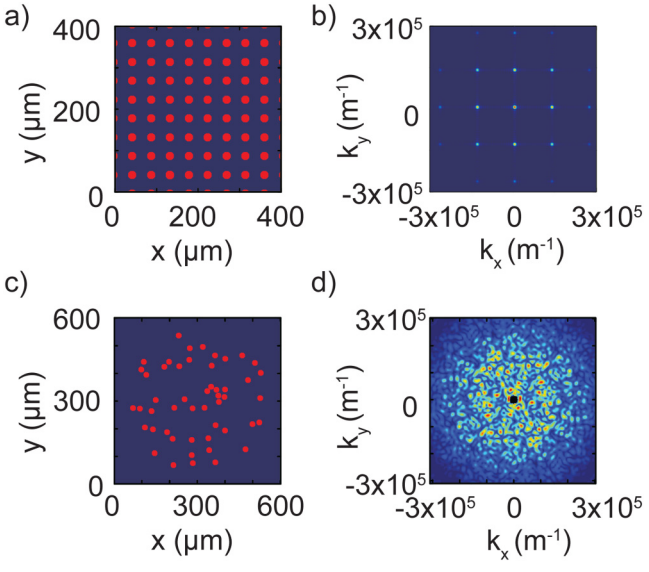

FIG. 1. (a) and (c) Dielectric environment $\epsilon(x)$ of ordered and random geometries of holes with 20 μm diameter which differ from the background in their refractive index. (b) and (d) Fourier space $|\epsilon(k)|$ obtained by two-dimensional Fourier transformation of $\epsilon(x)$. Ordered structures exhibit discrete peaks, while the random pattern contains a continuum of k-vectors.

depicted in Fig. 2, a small ($r = 5\,\mu$m) radius leads to continuous, broadly distributed Fourier components. With increasing scatter radius, the bandwidth and the homogeneity of the distribution decrease, while the maximum values of the occurring Fourier components increase. In the case of $r = 15\,\mu$m, pronounced lobes indicate a frequency selectivity due to the condition of no spatial overlap of the scatterers. Since a frequency nonselective feedback mechanism requires both broad and continuous and, at the same time sufficiently strong, k-values, a radius of 10 μm represents a good trade-off. To investigate the bandwidth of resonator structures experimentally, we investigate passive gold surfaces in transmission geometry in two ways: first, using a Fourier transformation infrared spectrometer (FTIR) and second, by time domain spectroscopy (TDS). By using the FTIR, we obtain information of spectrally resolved transmission over a spectral range of 1–6 THz with a resolution of 0.075 cm^{-1}. However, since we use the internal globar as the illumination source, the low signal-to-noise ratio does not allow a detailed resolution of occurring features in the spectrum but gives an overview of occurring resonances. To overcome this problem, we investigate the spectral range of interest, which contains the transmission features of ordered arrangements, using a TDS system that offers a better signal-to-noise ratio from 0.5 to 3.5 THz and time gating that prevents the detection of multiple reflections. The probing THz radiation (from 85 to 600 μm) is emitted by a large area photoconductive antenna,[20,21] excited at 780 nm, and recorded via electro-optic-detection[22,23] at 1560 nm. Both beams are provided by a custom MENLO femtosecond laser system with a two-color output (1560 and 780 nm). TDS is ideally suited for these measurements since it allows the distinction of direct transmission from multiple reflections at the sample interfaces. The samples, patterned gallium arsenide (GaAs) substrates, are fabricated by standard optical lithography, Au layer deposition, and a lift-off process. We fabricate three different samples consisting of subwavelength holes, with a diameter of 20 μm, arranged in square, hexagonal, and random geometries [Fig. 3(a)]. The overall sample area hereby exceeds the focal beam spot by at least a factor of two to prevent any effect from the boundaries of the patterned structure. In contrast to double-metal structures that completely block all radiation, the measurement of thin gold layers allows the determination of spectrally resolved transmission. Although active devices, fabricated in double-metal waveguides, show a three-dimensional geometry, results of two-dimensional models are in good approximation.[24] For periodic surfaces of subwavelength apertures, we expect the phenomenon of extraordinary optical transmission (EOT),[25] which yields frequency dependent transmission features determined by the array period. The EOT phenomena are linked to surface plasmons (SPs), oscillations of surface charges, which can be present on both sides of the metallic interface and must obey momentum conservation. The wavelength for a SPP on a flat metal-dielectric interface is given by where the wavelength of the excitation light in vacuum is and where the dielectric permittivities of the metal and dielectric are, respectively. In the case of a rectangular lattice, the Bragg-condition for resonance is given by $k_{SPP} = 2\pi\sqrt{\frac{i^2}{a^2} + \frac{j^2}{b^2}}$, where a and b are the x and y direction periodicities of the array and i and j are the whole number resonance orders along the x and y directions. For the given geometries, the frequencies of the

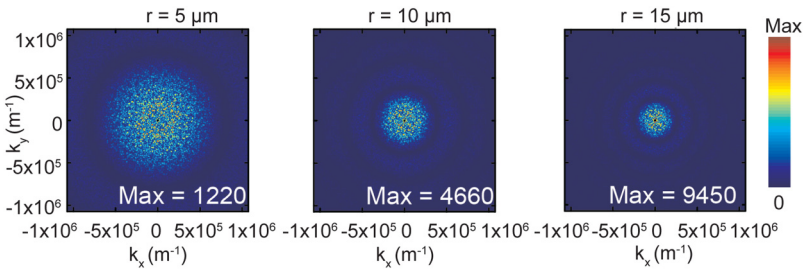

FIG. 2. Influence of the scatter radius. The Fourier spaces $|\epsilon(k)|$ of arrangements with fixed positions and varying scatter radii are depicted. With increasing scatter radius, the bandwidth and the homogeneity decrease, while the maximum values of the occurring Fourier component increases. To achieve frequency nonselective but strong feedback, a radius of 10 μm was selected for active devices.

GaAs-metal SPs, taking into account $n_{GaAs} = 3.6$ according to Ref. 26, correspond to 1.81 THz for the square ($a = 46\,\mu$m) lattice for the first order resonance under normal incidence. In Fig. 3, the spectrally resolved transmission obtained by FTIR and TDS is shown. As a reference for FTIR measurements, transmission data from GaAs without structured gold are included in the plots. The transmission is geometry dependent: Circles with a diameter of 20 μm arranged in hexagonal lattice show a transmission peak at 2.05 THz and at 1.81 ($i = 1, j = 0$) and 2.55 THz ($i = 1, j = 1$) for an arrangement in a square lattice with $a = 46\,\mu$m [Figs. 3(b) and 3(d)]. In contrast to the periodic patterns, the random pattern [Figs. 3(c) and 3(e)] shows no distinct transmission feature but a flat transmission increase over a broad spectral range. The increased transmission is a feature of the holes themselves and is expected to scale according to

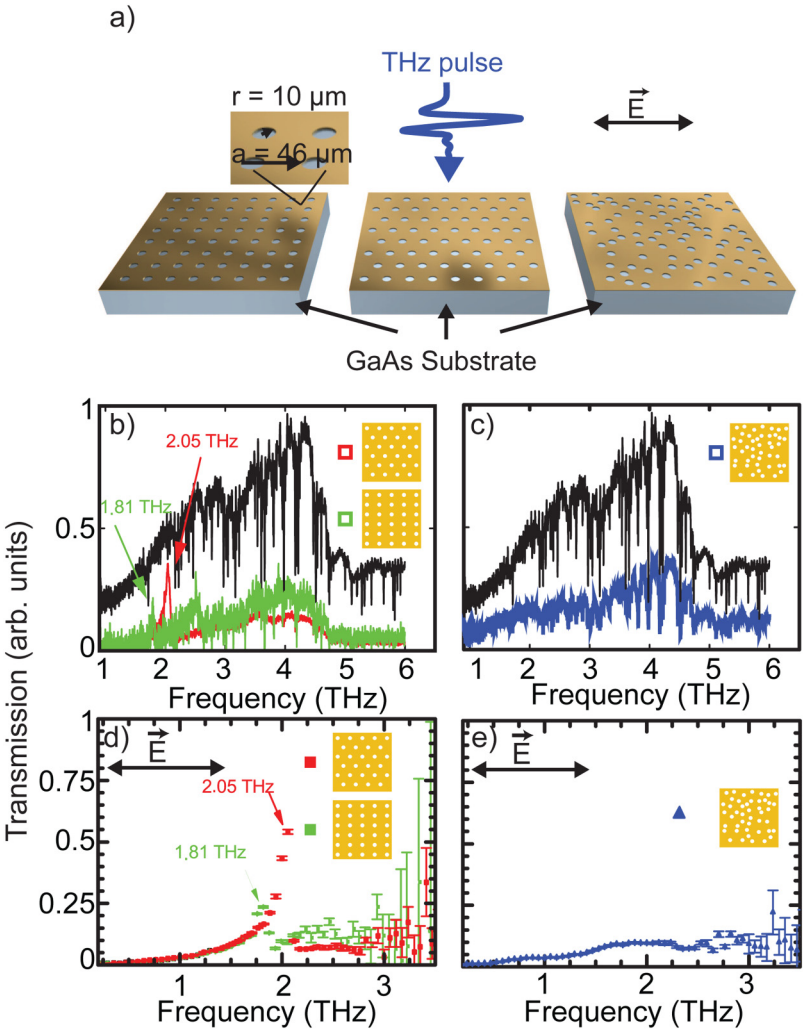

FIG. 3. (a) Schematic of prepared samples for measurements: square, hexagonal, and random patterned gold on the undoped GaAs substrate. The random pattern is created using a random number generator with the condition of no spatial overlap of the individual scattering centers, measured using an FTIR and a THz time domain spectroscopy setup. (b) and (c) Transmission of structured gold on undoped GaAs using the FTIR: periodic structures with peaks in the transmission spectra at corresponding plasmon frequencies for hexagonal lattice (red) and square lattice (green). The reference spectrum of unpatterned GaAs is depicted in black. Absorption lines originate from H_20 inside the beam path/FTIR. (d) and (e) Transmission of structured gold on undoped GaAs using TDS: Transmission spectra of periodic and random structures can be normalized to a GaAs reference due to higher S/N ratio. The spectra show resonances for ordered structures and a flat transmission response for random structures.

Bethe's theory for an infinitely thin perfect conductor.[27] However, real surfaces have a finite height and may deviate from perfect conductivity, which can result in higher transmission intensities and directionality.[28] Our measurements confirm the assumptions about the transmission behavior of structured and random pattern: Ordered structures exhibit the phenomenon of EOT with discrete peaks in the transmission spectrum, while a randomly arranged pattern manifests in a flat, nonfrequency selective response. Therefore, one can exclude that lasing spectra from active devices are not dominated by cavity inherited features but provide a spectrum corresponding only to the gain of the active region. Consequently, this feedback mechanism is applied to active devices.

III. MULTIPLE SCATTERING FOR RANDOM LASING

To investigate the mechanisms of the mode formation process induced by multiple scattering in THz QC random lasers, we have fabricated devices with double-metal waveguide geometries. In these waveguides, the active region is enclosed between two gold layers, which guide the mode and serve as electrical contacts. The necessary scattering for random lasing is implemented in two ways: (1) structuring the top gold electrode with a random pattern of circular openings, which leads to weak scattering and (2) etching cylindrical holes through the whole active region to strengthen the scattering [Fig. 4(a) left and right panels, respectively]. Both types of scattering rely on changes in the refractive index at the openings and the etched holes. To demonstrate the importance of the scattering strength, 3D finite element method calculations to solve Maxwell's equation were performed. The same scattering configuration was simulated twice: once with structured top gold layer ("top gold") and once with perforated active region ("etched"), and the mode with the lowest effective loss $\alpha = \frac{2\pi n \nu}{c Q_{factor}}$, with refractive index n, frequency ν, quality factor Q, and speed of light c, was selected. The results are depicted in Fig. 4(b): both simulations result in modes with similar field distribution; however, stronger scattering, due to a larger difference in refractive index, leads to a lower loss of the mode. For the simulations and experimental devices, the positions of the scattering centers are selected using a random number generator with the condition of no spatial overlap of holes. To study lasing based on feedback by multiple scattering for these two different structures, an active region sensitive to optical losses is used.[29] It consists of a three-well structure based on the GaAs/$Al_xGa_{1-x}As$ material system [see Fig. 4(c)] with 195 cascades which result in an active region thickness of 12.5 μm. To achieve high temperature operation, the active region has high barriers ($x = 0.24$) to suppress thermal leakage of the carriers and a diagonal optical transition to increase the upper-state lifetime.[29,30] The diagonality of the optical transition can be expressed by the oscillator strength f_{ul}, where a low oscillator strength describes a small overlap of the wave functions involved in the lasing transition. Photon-assisted tunneling in semiconductor heterostructures opens a current-carrying channel and is related to the optical transition rate W_{ul} of the stimulated transition. It is therefore proportional to $(f_{ul})^2$.[31] The interplay between this photon-assisted tunneling current and nonradiative scattering processes is necessary for a stable operation of the QC structure. The very low oscillator strength $f_{ul} = 0.22$ of the used structure results in electrical instabilities, in the case of lossy resonators, which are described in detail in Ref. 32. Comparable designs from Kumar *et al.*[30] and Fathololoumi *et al.*[6] have values of $f_{ul} = 0.38$ and $f_{ul} = 0.47$, respectively.

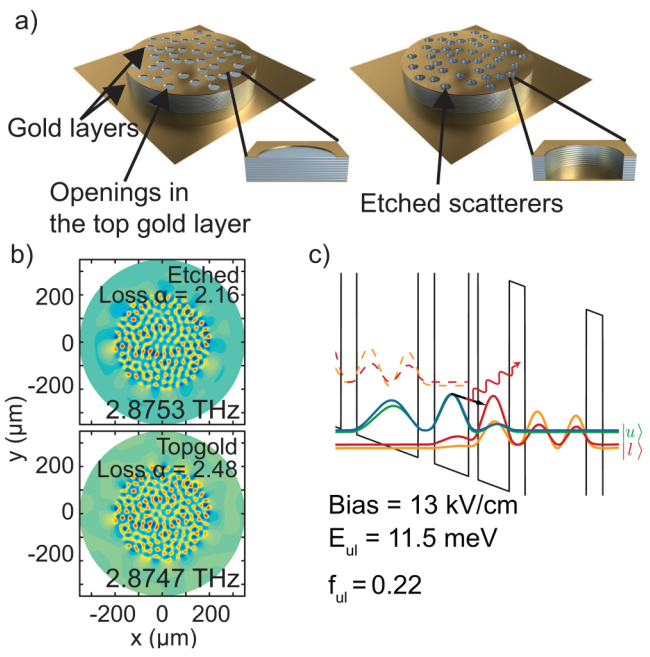

FIG. 4. (a) Schematic of device with structured top electrode (left) and etched device (right). The mode is confined between two gold layers (metal–metal waveguide). The diameter of the devices is 400 μm and the diameter of the scatterers 20 μm. (b) 3D FEM calculations of structured top gold and etched scatterers: Using the same scattering configuration both simulations exhibit similar modes with lower loss for etched scatterers. (c) Band structure of the used GaAs/$Al_{0.24}Ga_{0.76}As$ active region. Upper and lower laser levels have an energy difference of 11.5 meV and an oscillator strength of 0.22.

This new active region is ideally suited to study the mode confinement in the heterostructure, as too high losses reduce the photon density inside the cavity. This leads to a weaker role of the photon-assisted transport (via stimulated emission) of electrons through the quantum cascade heterostructure and the lasing threshold is shifted or cannot be reached at all. Only cavities providing feedback by multiple-photon scattering that is strong enough to compensate for losses introduced by the perturbation of the metal–metal waveguide will maintain a photon density high enough to stabilize the carrier transport. We use this feature to prove that modes formed inside the resonator geometries in Fig. 4(a) are indeed formed by multiple scattering and not just outcoupled radiation originating from whispering gallery modes of disk-shaped resonators. To probe the scattering strength, devices in disk shape with a diameter of 400 μm and a scatter diameter of 20 μm and with the same scattering configuration (same filling fraction and position of scatterers) are processed in two batches: one with a structured top gold electrode and one with cylindrical holes etched into the active region down to the bottom contact. With each batch, unstructured reference devices are processed to exclude processing related issues.

The processed THz QCL chips are mounted into a flow cryostat and operated in the pulsed operation mode, using rectangular 1 μs long pulses with a repetition rate of 10 kHz (corresponding to 1% duty cycle). The light emitted from the QCLs is coupled to a FTIR via a collimating parabolic mirror. In Fig. 5(a), Light–Current–Voltage (L–I–V) characteristics of different cavities are compared. The unstructured device in disk shape(diameter 400 μm) emits from the rim and is depicted as a reference. The I–V curves demonstrate the robustness of QC active regions. The modification of the scattering strength is possible without deterioration of the gain. Devices with structured top gold electrode (weak scattering) and 8% filling fraction do not show lasing operation. This is due to the increased waveguide losses. However, devices with an 8% filling fraction, same scatter coordinates but etched pillars (strong scattering) exhibit a different behavior as the spectrum in Fig. 5(b) shows. Because of the large contrast between the refractive index of air and the GaAs heterostructure, etched pillars provide feedback which is strong enough to support modes with a sufficiently high Q-factor to allow laser operation. The multiple scattering at the etched holes enables strong mode confinement and allows the transition into the lasing regime. The results from devices with different types of scatterers directly show the influence of the scattering strength. In the case of etched pillars, the losses originating from the pillars and the opening of the top gold are compensated by the feedback provided by the multiple scattering. We therefore conclude that the modes of random lasers are indeed influenced and formed by the multiple scattering when the scatterers are placed randomly. In Fig. 5(b), the spectrum of the lasing modes covers a bandwidth of approx. 350 GHz. In comparison, the QCL device with unstructured disk emits at frequencies corresponding to whispering gallery modes which are spaced by 30 GHz and covers approx. 100 GHz spectral range. In the case of the random laser devices, we exclude whispering gallery modes, since the holes cover the entire resonator surface and force the modes to scatter. Furthermore, different scatter positions lead to different spectra.[14] We conclude that the spectral limitations in the case of the random pattern originate from the used active region and not from the resonator design.

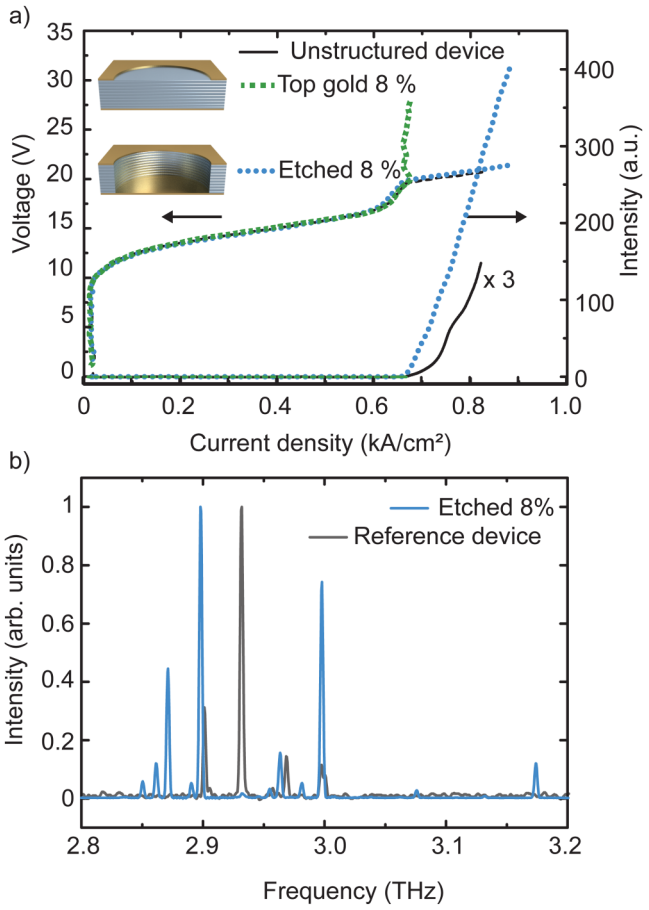

FIG. 5. (a) Light-Current-Voltage characteristics of 8 filling fraction devices with structured top gold electrode and etched devices. The unstructured device in disk shape with a diameter of 400 μm, emitting from the facet, is depicted as reference. (b) Spectra of device with etched pillars and 8% filling fraction and reference device (unperturbed disk with 400 μm diameter), measured with FTIR in pulsed mode.

IV. CONCLUSION

We have investigated the feedback mechanism by multiple scattering at randomly placed scatterers. We have demonstrated the influence of the radius of the individual scatterers. We find that the radius must be chosen correctly to get reasonable feedback strength while maintaining a large bandwidth. Experimentally, we have investigated the bandwidth and frequency selectivity of different cavity geometries by measuring the spectrally resolved transmission through test structures. We find a frequency nonselective, flat response for random arrangements. In contrast, ordered structures in hexagonal or square lattice show distinct transmission features. We have fabricated active lasing devices and probed the scattering strength of different types of scatterers. Due to the used waveguide concept and a specific active region, we can determine the origin of the lasing modes. We demonstrate that all outcoupled modes are the result of multiple-photon scattering in a random resonator. In conclusion, we answer two fundamental questions concerning the applied multiple scattering feedback mechanism. It is perfectly suited for broadband emission due to its frequency nonselective nature. By carefully designing the shape of the scatterer, the feedback strength can be adjusted. Finally, we confirm that lasing spectra from active random lasers devices are not dominated by cavity inherited features but depend on the gain characteristics of the active region and the scattering strength. Both findings are important for the further development of broadband lasers. For applications in imaging and spectroscopy, the increase of the lasing bandwidth is desired. This can be achieved by realizing broadband active regions and by designing advanced scattering patterns with different geometries and scattering strength.

ACKNOWLEDGMENTS

The authors acknowledge financial support received by the Austrian Science Fund (FWF) through Project Nos. P30709 (DiPQCL), W1210 (DK CoQuS), W1243 (DK Solids4Fun), and FFG Project

No. 849614 (COMTERA). This work was supported by the ESF under Project No. CZ.02.2.69/0.0/0.0/16_027/0008371.

REFERENCES

[1]C. Walther, M. Fischer, G. Scalari, R. Terazzi, N. Hoyler, and J. Faist, "Quantum cascade lasers operating from 1.2 to 1.6 THz," Appl. Phys. Lett. **91**, 131122 (2007).
[2]M. Wienold, B. Röben, X. Lü, G. Rozas, L. Schrottke, K. Biermann, and H. T. Grahn, "Frequency dependence of the maximum operating temperature for quantum-cascade lasers up to 5.4 THz," Appl. Phys. Lett. **107**, 202101 (2015).
[3]M. Rösch, G. Scalari, M. Beck, and J. Faist, "Octave-spanning semiconductor laser," Nat. Photonics **9**, 42–47 (2015).
[4]L. Li, L. Chen, J. Freeman, M. Salih, P. Dean, A. Davies, and E. Linfield, "Multi-Watt high-power THz frequency quantum cascade lasers," Electron. Lett. **53**, 799–800 (2017).
[5]X. Wang, C. Shen, T. Jiang, Z. Zhan, Q. Deng, W. Li, W. Wu, N. Yang, W. Chu, and S. Duan, "High-power terahertz quantum cascade lasers with 0.23 W in continuous wave mode," AIP Adv. **6**, 075210 (2016).
[6]S. Fathololoumi, E. Dupont, C. W. I. Chan, Z. R. Wasilewski, S. R. Laframboise, D. Ban, A. Mátyás, C. Jirauschek, Q. Hu, and H. C. Liu, "Terahertz quantum cascade lasers operating up to 200 K with optimized oscillator strength and improved injection tunneling," Opt. Express **20**, 3866–3876 (2012).
[7]E. Mujagić, C. Deutsch, H. Detz, P. Klang, M. Nobile, A. M. Andrews, W. Schrenk, K. Unterrainer, and G. Strasser, "Vertically emitting terahertz quantum cascade ring lasers," Appl. Phys. Lett. **95**, 011120 (2009).
[8]S. Biasco, K. Garrasi, F. Castellano, L. Li, H. E. Beere, D. A. Ritchie, E. H. Linfield, A. G. Davies, and M. S. Vitiello, "Continuous-wave highly-efficient low-divergence terahertz wire lasers," Nat. Commun. **9**, 1122 (2018).
[9]Y. Chassagneux, R. Colombelli, W. Maineult, S. Barbieri, H. E. Beere, D. A. Ritchie, S. P. Khanna, E. H. Linfield, and A. G. Davies, "Electrically pumped photonic-crystal terahertz lasers controlled by boundary conditions," Nature **457**, 174–178 (2009).
[10]M. S. Vitiello, M. Nobile, A. Ronzani, A. Tredicucci, F. Castellano, V. Talora, L. Li, E. H. Linfield, and A. G. Davies, "Photonic quasi-crystal terahertz lasers," Nat. Commun. **5**, 5884 (2014).
[11]R. Degl'Innocenti, Y. D. Shah, L. Masini, A. Ronzani, A. Pitanti, Y. Ren, D. S. Jessop, A. Tredicucci, H. E. Beere, and D. A. Ritchie, "Hyperuniform disordered terahertz quantum cascade laser," Sci. Rep. **6**, 19325 (2016).
[12]Y. Zeng, G. Liang, H. K. Liang, S. Mansha, B. Meng, T. Liu, X. Hu, J. Tao, L. Li, A. G. Davies, E. H. Linfield, Y. Zhang, Y. Chong, and Q. J. Wang, "Designer multimode localized random lasing in amorphous lattices at terahertz frequencies," ACS Photonics **3**, 2453–2460 (2016).
[13]Y. Zeng, G. Liang, B. Qiang, K. Wu, J. Tao, X. Hu, L. Li, A. G. Davies, E. H. Linfield, H. K. Liang, Y. Zhang, Y. Chong, and Q. J. Wang, "Two-dimensional multimode terahertz random lasing with metal pillars," ACS Photonics **5**, 2928–2935 (2018).
[14]S. Schönhuber, M. Brandstetter, T. Hisch, C. Deutsch, M. Krall, H. Detz, A. M. Andrews, G. Strasser, S. Rotter, and K. Unterrainer, "Random lasers for broadband directional emission," Optica **3**, 1035 (2016).
[15]B. Redding, M. A. Choma, and H. Cao, "Speckle-free laser imaging using random laser illumination," Nat. Photonics **6**, 355–359 (2012).
[16]B. Redding, A. Cerjan, X. Huang, M. L. Lee, A. D. Stone, M. A. Choma, and H. Cao, "Low-spatial coherence electrically-pumped semiconductor laser for speckle-free full-field imaging," PNAS **112**(5), 1304 (2015).
[17]M. Segev, Y. Silberberg, and D. N. Christodoulides, "Anderson localization of light," Nat. Photonics **7**, 197–204 (2013).
[18]S. Esterhazy, D. Liu, M. Liertzer, A. Cerjan, L. Ge, K. G. Makris, A. D. Stone, J. M. Melenk, S. G. Johnson, and S. Rotter, "Scalable numerical approach for the steady-state *ab initio* laser theory," Phys. Rev. A **90**, 023816 (2014).
[19]C. L. Tang, H. Statz, and G. deMars, "Spectral output and spiking behavior of solid-state lasers," J. Appl. Phys. **34**, 2289–2295 (1963).
[20]D. H. Auston, K. P. Cheung, and P. R. Smith, "Picosecond photoconducting Hertzian dipoles," Appl. Phys. Lett. **45**, 284–286 (1984).
[21]A. Dreyhaupt, S. Winnerl, T. Dekorsy, and M. Helm, "High-intensity terahertz radiation from a microstructured large-area photoconductor," Appl. Phys. Lett. **86**, 121114 (2005).
[22]Q. Wu and X.-C. Zhang, "Design and characterization of traveling-wave electrooptic terahertz sensors," IEEE J. Sel. Top. Quantum Electron. **2**, 693–700 (1996).
[23]A. Leitenstorfer, S. Hunsche, J. Shah, M. C. Nuss, and W. H. Knox, "Detectors and sources for ultrabroadband electro-optic sampling: Experiment and theory," Appl. Phys. Lett. **74**, 1516–1518 (1999).
[24]M. Krall, "Nanoscale transport and photonic confinement in terahertz quantum cascade lasers," dissertation (Photonics Institute, TU Wien, Austria, 2016).
[25]T. W. Ebbesen, H. J. Lezec, H. F. Ghaemi, T. Thio, and P. A. Wolff, "Extraordinary optical transmission through sub-wavelength hole arrays," Nature **391**, 667–669 (1998).
[26]*Handbook of Optical Constants of Solids*, edited by E. D. Palik, (Academic Press, 1998), Vol. 3.
[27]H. A. Bethe, "Theory of diffraction by small holes," Phys. Rev. **66**, 163–182 (1944).
[28]A. Degiron, H. Lezec, N. Yamamoto, and T. Ebbesen, "Optical transmission properties of a single subwavelength aperture in a real metal," Opt. Commun. **239**, 61–66 (2004).
[29]M. A. Kainz, S. Schönhuber, A. M. Andrews, H. Detz, B. Limbacher, G. Strasser, and K. Unterrainer, "Barrier height tuning of terahertz quantum cascade lasers for high-temperature operation," ACS Photonics **5**, 4687–4693 (2018).
[30]S. Kumar, C. W. I. Chan, Q. Hu, and J. L. Reno, "Two-well terahertz quantum-cascade laser with direct intrawell-phonon depopulation," Appl. Phys. Lett. **95**, 141110 (2009).
[31]H. Liu and F. Capasso, *Intersubband Transitions in Quantum Wells: Physics and Device Applications II* (Academic Press, San Diego, 2000).
[32]S. Fathololoumi, E. Dupont, Z. R. Wasilewski, C. W. I. Chan, S. G. Razavipour, S. R. Laframboise, S. Huang, Q. Hu, D. Ban, and H. C. Liu, "Effect of oscillator strength and intermediate resonance on the performance of resonant phonon-based terahertz quantum cascade lasers," J. Appl. Phys. **113**, 113109 (2013).